ISSN 1392–1320 MATERIALS SCIENCE (MEDŽIAGOTYRA). Vol. 16, No. 4. 2010

Structural and Dielectric Properties of $(Bi_{1/2}Na_{1/2})TiO_3$-WO_3 Ceramics

Kamini KUMARI, Ashutosh PRASAD, Kamal PRASAD *

University Department of Physics, T. M. Bhagalpur University, Bhagalpur, 812 007, India

Received 12 April 2010; accepted 29 May 2010

Polycrystalline samples of lead-free $(1–x)(Bi_{1/2}Na_{1/2})TiO_3$-$xWO_3$ with $(0 \le x \le 0.10)$ were prepared using a high-temperature solid-state reaction method. X-ray diffraction analyses indicated the formation of single-phase orthorhombic structure. It is seen that addition of WO_3 to $(Bi_{1/2}Na_{1/2})TiO_3$ changes the crystal symmetry. Williamson-Hall approach was applied to estimate the apparent particle size and lattice strain of the compounds. The values of apparent particle size and lattice strain are seen to increase with the increasing WO_3 content. Temperature dependence of dielectric constant showed that the addition of WO_3 to $(Bi_{1/2}Na_{1/2})TiO_3$ shifts phase transition temperature as well as depolarization temperature to higher temperature side. Permittivity data showed a low temperature coefficient of capacitance ($T_{CC} < 4$ %) up to 100 °C.

Keywords: lead-free, $(Bi_{1/2}Na_{1/2})TiO_3$, ceramic, dielectric properties, diffuse phase transition.

1. INTRODUCTION

Bismuth sodium titanate, $(Bi_{1/2}Na_{1/2})TiO_3$ (BNT) is considered to be an excellent key lead-free piezoelectric ceramic material, which shows strong ferroelectric properties [1 – 5]. BNT has a Curie temperature (T_m = 320°C) and large remanant polarization (P_r = 38 μC/cm^2). In addition, BNT exhibits an anomaly in its dielectric properties as a result of low temperature phase transition from ferroelectric to anti-ferroelectric phase at about 200°C. This temperature is termed as depolarization temperature T_d. This T_d is an important factor for BNT and BNT-based ceramics in view of their practical uses, because the piezoelectric response disappears above T_d [6 – 8]. Further, the materials used for piezoelectric applications are mainly lead bearing compounds, e. g. $Pb(Zr,Ti)O_3$, $Pb(Mg_{1/3}Nb_{2/3})O_3$, $PbTiO_3$, etc. Recently the legislation on waste electrical/electronic equipment has been issued by the EU. Since 2006 use of hazardous lead and lead bearing substances in electrical parts have been prohibited. In order to meet this requirement, a search for alternative environment friendly lead-free materials has become the global concern. The electronic structure of different components of $(Bi_{1/2}Na_{1/2})TiO_3$ and $Pb(Zr,Ti)O_3$ are: Bi (Z = 83) [(Xe)$6s^2 4f^{14} 5d^{10} 6p^3$]; Na ($Z$ = 11) [(Ne)$3s^1$]; Ti (Z = 22) [(Ar)$4s^2 3d^2$]; O (Z = 8) [(He)$2s^2 2p^4$]; Pb (Z = 82) [(Xe)$6s^2 4f^{14} 5d^{10} 6p^2$] and Zr ($Z$ = 40) [(Kr)$5s^2 4d^2$]. The covalency between unoccupied states of the A-site ion in the perovskite structure, such as Pb 6d-states and Bi 6d-states, and O p-states favoured ferroelectric ground states [8 – 10].

The fact that Bi^{3+} ions are isoelectronic with Pb^{2+}, both showing a lone pair effect attracted world-wide attention of researchers for further studies of BNT as an alternative to PZT ceramics. Besides, it has been reported that the additives like $MnCO_3$ [11], La_2O_3 [12,13], CeO_2 [13], ZrO_2 [14], Bi_2O_3-Sc_2O_3 [15], $LiTaO_3$ [16], $NaNbO_3$ [17], $BaNb_2O_6$ [18], $ZnNb_2O_6$ [19], etc. showed improvement in the electrical properties of BNT while the T_d was greatly reduced. Recent studies have shown T_d and T_m at 300°C and 438°C, respectively at 1 kHz, thus showing a shift in both the temperatures towards higher side [20]. In view of the above, the system $(1–x)$BNT-xWO_3 deserved further investigation. Accordingly, structural, microstructural, and dielectric properties of $(1–x)$BNT-xWO_3 ceramic system with $(0 \le x \le 0.10)$ have been reported in the present work.

2. EXPERIMENTAL

A conventional ceramic fabrication technique was adopted in order to prepare WO_3 added $(Bi_{1/2}Na_{1/2})TiO_3$ ceramics with x = 0, 0.025, 0.050, 0.075 and 0.10 using AR-grade (99.9 % + pure) chemicals (Bi_2O_3, Na_2CO_3, TiO_2 and WO_3). The optimized calcination and sintering temperatures were respectively kept at 1050 °C for 4 h and 1090 °C for 3 h under oxygen atmosphere. The detailed preparation conditions are discussed in the literature [20]. The XRD data were taken on calcined powder with a X-ray diffractometer (Siemens D500) at room temperature, using CoK_α radiation (λ = 1.7902 Å), over a wide range of Bragg angles ($20° \le 2\theta \le 80°$) with a scanning speed of 2° min^{-1}. The microstructure of the fractured surface of sintered BNT-WO_3 was analysed using a computer controlled scanning electron microscope (JEOL-JSM840A). The frequency dependent complex dielectric constant, $\varepsilon^* (= \varepsilon' - i\varepsilon'')$, phase angle ($\theta$) and loss tangent (tan$\delta$) were measured as a function of frequency at different temperatures using a computer-controlled LCR Hi-Tester (HIOKI 3532-50, Japan) attached with a microprocessor controlled dry temperature controller (DPI-1100, Sartech Intl., India) on a symmetrical cell of type Ag|ceramic|Ag, where Ag is a conductive paint coated on either side of the pellet. The thicknesses of BNT-WO_3 ceramic samples, sandwiched between the Ag electrodes were 0.97 mm, 1.15 mm, 1.52 mm, 1.28 mm and 1.23 mm for x = 0, 0.025, 0.050, 0.075 and 0.10, respectively.

*Corresponding author. Tel.: +91-641-2501699; fax: +91-641-2501699.
E-mail address: *k.prasad65@gmail.com* (K. Prasad)

3. RESULTS AND DISCUSSION

Fig. 1 shows the XRD-profile of BNT-WO_3 at room temperature. A standard computer program (POWD) was utilized for the XRD-profile analysis. A good agreement between the observed ($d_{obs} = \lambda / 2\sin\theta$) and calculated ($d_{calc} = 1/\sqrt{h^2/a^2 + k^2/b^2 + l^2/c^2}$) interplanar spacings were found, thereby suggesting the formation of single-phase compounds. It is well known that BNT has a rhombohedral crystal structure and the addition of WO_3 to BNT ceramics has produced orthorhombic phase. Therefore, the addition of WO_3 to BNT is supposed to alter the crystal symmetry from rhombohedral to orthorhombic [20]. The appearance of an additional peak (121) and its regular growth in intensity in BNT-WO_3 compositions with the increase in WO_3 content may presumably be due to replacement of pseudocation ($Na_{1/2}Bi_{1/2}$) at the A-site by tungsten ion, which may have led to the appearance of dominant orthorhombic phase of WO_3 by suppressing rhombohedral phase of BNT. The criterion for reliability of evaluation and indexing for the structure of BNT-WO_3 is to get a minimum value for the sum of differences in observed and calculated *d*-values [i.e. $\sum \Delta d = \sum (d_{obs} - d_{calc})$]. The refined structural parameters for all the compositions along with their unit cell volume ($a \times b \times c$) are illustrated in Fig. 2.

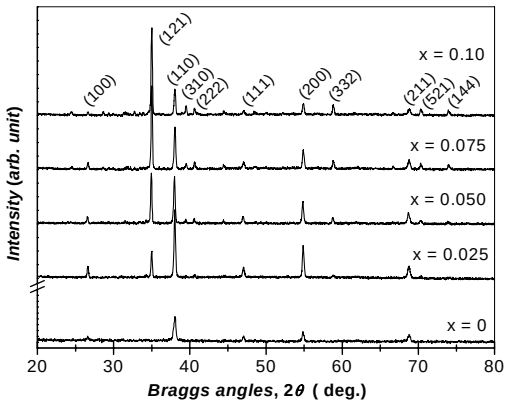

Fig. 1. X-ray diffraction pattern of $(1–x)(Bi_{1/2}Na_{1/2})TiO_3$-$xWO_3$ at room temperature

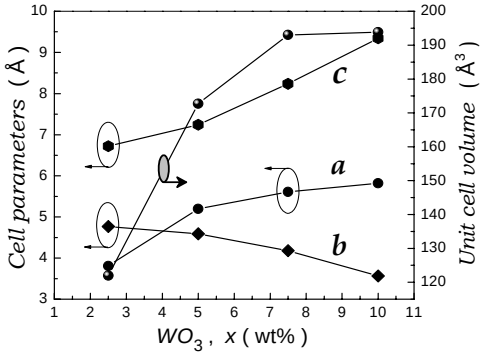

Fig. 2. Variation of lattice parameters and unit cell volume with WO_3 content

It is observed that the values of *a* as well as *c* increase while the value of *b* decreases with the increasing WO_3 content. Also an increase in the unit cell volume has been observed with the increment in additive percentage. The apparent particle size and lattice strain of BNT-WO_3 were estimated by analyzing the X-ray diffraction peak broadening, using Williamson-Hall approach [21]:

$$\beta\cos\theta = (K\lambda / D) + 2(\Delta\xi / \xi)\sin\theta, \quad (1)$$

where *D* is the apparent particle size, β is the full width at half diffraction intensity maximum (FWHM) and $\Delta\xi / \xi$ is the lattice strain, *K* is the Scherrer constant (0.89). The term $K\lambda/D$ represents the Scherrer particle size distribution. The lattice strain can be estimated from the slope of $\beta\cos\theta/\lambda$ versus $\sin\theta/\lambda$ plot and the apparent particle size can be estimated from the intersection of this line at $\sin\theta = 0$. Linear least square fitting to $\beta\cos\theta/\lambda - \sin\theta/\lambda$ data provided the values of intercept and slope of the plots. A Gaussian model was applied to estimate FWHM.

$$I = I_o + (A / \beta\sqrt{\pi / 2}) \exp[-2\{(\theta - \theta_c) / \beta\}^2], \quad (2)$$

where *A* and θ_c are respectively the area and centre of the curve. Fig. 3 illustrates the Williamson-Hall plot for BNT-WO_3 and Inset shows the variation of apparent particle size and lattice strain with the increasing WO_3 content. It can be seen that the values of apparent particle size and lattice strain, both, generally increase with the increasing WO_3 content. Besides, the lattice strain is found to be maximum for the composition $x = 0.075$.

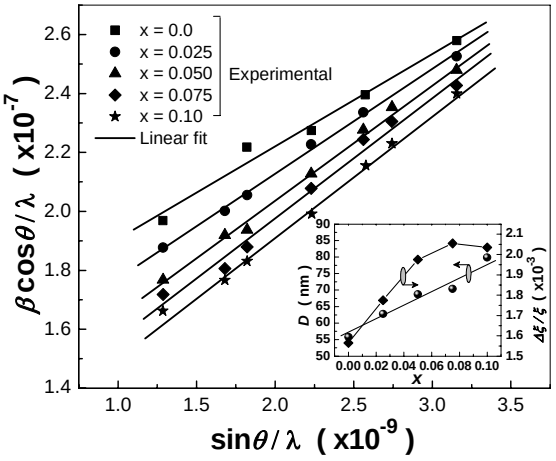

Fig. 3. Williamson-Hall plots for $(1–x)(Bi_{1/2}Na_{1/2})TiO_3$-$xWO_3$. Inset: Variation of apparent particle size and strain coefficient with WO_3 content (*x*)

Figs. 4 (a – d) show the SEM-micrographs of BNT-WO_3 at 1 μm scale. The grains of unequal sizes (~1 – 3 μm) appear to be distributed throughout the sample. The ratio of the apparent particle size to the grain size of BNT-WO_3 is found to be of the order of 10^{-2}.

Figs. 5 and 6, respectively, show the frequency dependence of real and imaginary parts of dielectric constant (ε' and ε'') at different temperatures. It is observed that ε' follows inverse dependence on frequency, normally followed by almost all dielectric/ferroelectric materials. Also, the value of ε'' decreases with increase in frequency in the low temperature region, while at higher temperatures,

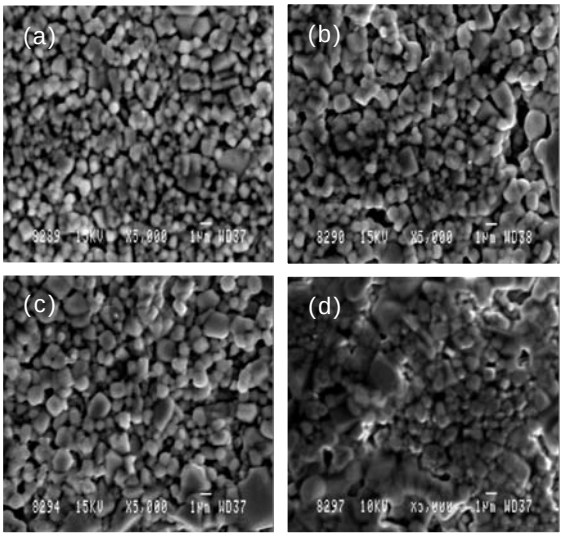

Fig. 4. SEM micrographs of $(1–x)(Bi_{1/2}Na_{1/2})TiO_3$-$xWO_3$: a – x = = 0.025; b – x = 0.05; c – x = 0.075; d – x = 0.10

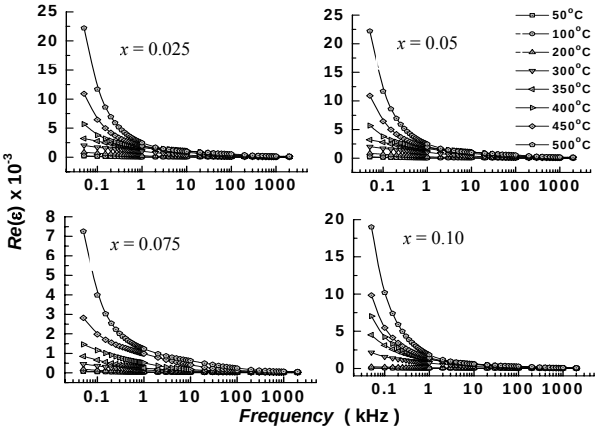

Fig. 5. Variation of real part of dielectric constant (ε') with frequency at different temperatures for $(1–x)(Bi_{1/2}Na_{1/2})$ TiO_3-xWO_3 ceramics

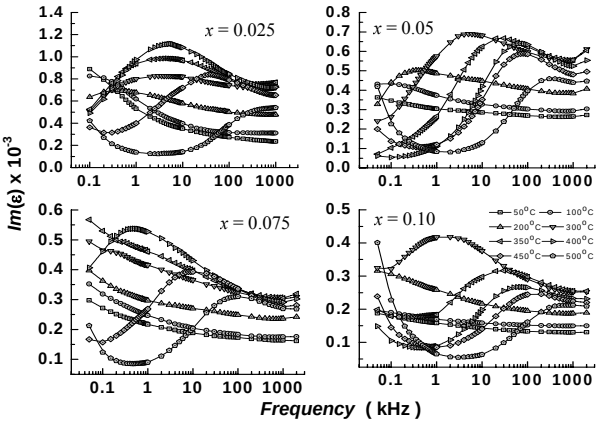

Fig. 6. Variation of imaginary part of dielectric constant (ε'') with frequency at different temperatures for $(1–x)(Bi_{1/2}Na_{1/2})$ TiO_3-xWO_3 ceramics

it reaches a maximum, shifting towards higher frequency side. Dispersion with relatively high dielectric constant can be seen in the ε'-f graph in the lower frequency region and the dielectric constant drops at high frequencies. This is due to the fact that dipoles can no longer follow the field at high frequencies. Further, it is well known that there is a pronounced effect of frequency as well as of temperature on the electrical conduction and dielectric relaxations in a material. The relationship between ε'' and σ is given by $\varepsilon'' = \sigma / \omega\varepsilon_o = (\sigma_d + \sigma_i) / \omega\varepsilon_o$, and consequently, the expression: $\varepsilon^* = \varepsilon' - i\varepsilon''$ may be rewritten as [22]:

$$\varepsilon^* = \varepsilon' - i(\varepsilon'' + \sigma_i / \omega\varepsilon_o) \,, \tag{3}$$

where σ_d and σ_i represent conductivity due to dipole relaxation and that due to ionic drift, respectively. It is evident from Fig. 6 that for all the compositions ε'' increases with the decrease in frequency at a given temperature and as the temperature is increased further, ε'' increased at a faster pace and with the increase in temperature, ionic relaxation part dominates over the dipolar part. Also, the relaxation peak (ε''_{max}) shifts towards higher frequencies with increasing temperature, thereby indicating the increasing loss in the sample for all the compositions. The most probable frequency $\omega_m (= 1/\tau_m)$ was obtained from the frequency at which ε''_{max} is observed. At the peak, the relaxation is defined as:

$$\omega_m \tau_m = 1, \tag{4}$$

where τ_m is the relaxation time. The most probable frequency follows the Arrhenius law given by:

$$\omega_m = \omega_0 \exp(-E_a / k_B T) \,, \tag{5}$$

where ω_0 is the pre-exponential factor and E_a is the activation energy. Fig. 7 shows a plot of $\log\omega_m$ *vs*. $1/T$. The activation energy E_a, for all compositions, estimated using least squares fit to the data points are shown in the inset of Fig. 7. The activation energy is found to be maximum for the composition $x = 0.075$.

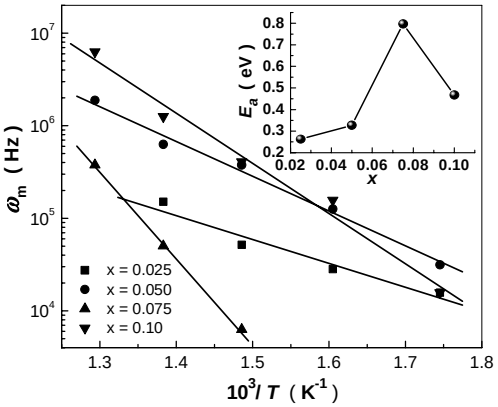

Fig. 7. Temperature dependence of most probable relaxation frequency for $(1–x)(Bi_{1/2}Na_{1/2})TiO_3$-$xWO_3$. The symbols are the experimental points and the solid line is the linear least squares fit. Inset: Variation of activation energy with WO_3 content (x)

The temperature dependence of dielectric constant (ε) and loss tangent ($\tan\delta$) at 1 kHz for BNT-WO_3 system are shown in Fig. 8. Inset of Fig. 8 shows the room temperature dielectric constant (ε_{RT}), dielectric constant maximum (ε_m) and corresponding temperature (T_m) as function WO_3 content in BNT solid solutions. It is seen that the addition of WO_3 to BNT shifts T_m as well as T_d to higher

temperature side in comparison to pure BNT (T_m = 320 °C and T_d = 200 °C). This shift in T_m and T_d towards high side in case of BNT and BNT-based solid solutions is apt for piezoelectric applications. Further, the value of T_m is found to be lower for $x = 0.075$ in comparison to other compositions (inset Fig. 8), which may be attributed to the fact that the values of activation energy and lattice strain are maximum for this composition. Also, the ε-T plots show a broad ferroelectric-paraelectric phase transition (i. e. diffuse phase transition, DPT). The broadening in the dielectric peak is a common phenomenon occurring in solid solutions. It has been observed that the multiple ion occupation at different sites, microstructure and sintering process cause deviation from normal Curie-Weiss behaviour, where T_m is not sharp, but physical properties change rather gradually over a temperature range. This type of phase transition is known as DPT. The DPT can be explained by modified Curie-Weiss law:

$$\ln(\varepsilon^{-1} - \varepsilon_m^{-1}) = \ln A + \gamma \ln(T - T_m), \quad (6)$$

where T is temperature, A is a constant and γ (diffusivity parameter) is the critical exponent which has a value equal to 1 for normal phase transition and it is 1–2 for DPT. A linear regression analysis of experimental data to Eqn. (6) yielded the value of $\gamma > 1$ for all the compositions, clearly indicating thereby the existence of DPT. The occurrence of DPT in BNT-WO_3 may be due to the presence of more than one cation in the sub-lattice that might have produced some kind of heterogeneities. Further, the temperature coefficient of capacitance (T_{CC}), an important parameter for the low-temperature dependence of capacitance, is defined as: $T_{CC}(\%) = [(C_T - C_{RT})/C_{RT}] \times 100$, where C_T and C_{RT} are the capacitances at a given temperature T and at room temperature (RT), respectively. It is important to note that a comparatively higher value of T_{CC} (= 17 %) was found for BNT while a low value of T_{CC} (< 4 %) up to 100 °C has been found for all the WO_3 added BNT compositions indicating thereby that BNT-WO_3 system may be a potential candidate for capacitor applications.

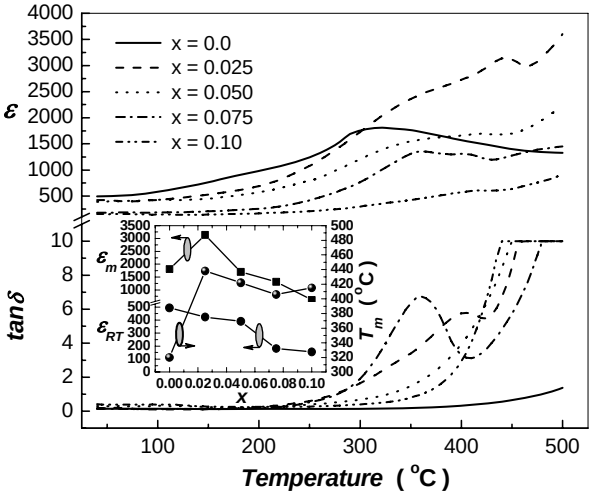

Fig. 8. Variation of dielectric constant and dielectric loss with temperature for (1-x)($Bi_{1/2}Na_{1/2}$)TiO_3-xWO_3 ceramics at 1 kHz. Inset: Variation of ε_{RT}, ε_m and T_m with WO_3 content (x)

4. CONCLUSION

Polycrystalline samples of BNT-WO_3, prepared through a high-temperature solid-state reaction technique, were found to have single-phase perovskite type orthorhombic structure. Therefore, the addition of WO_3 to BNT changes the crystal symmetry. The values of apparent particle size and lattice strain increase with the increasing WO_3 content. The addition of WO_3 to BNT shifts T_m as well as T_d to higher temperature side. The property of shifting in T_m and T_d towards higher side in ceramics is favourable for their piezoelectric applications. Further, permittivity data showed low temperature coefficient of capacitance (T_{CC} < 4 %) in the working temperature range, i. e. up to 100 °C.

Acknowledgements

The financial support, by the Department of Science and Technology, New Delhi (Grant No. SR/S2/CMP-17/2008) for the present work, is gratefully acknowledged. The authors also acknowledge S. Sen, CGCRI Kolkata, India for arranging XRD data and SEM of the samples.

REFERENCES

1. **Roleder, K., Suchanicz, J., Kania, A.** Time Dependence of Electric Permittivity in $Na_{0.5}Bi_{0.5}TiO_3$ Single Crystals *Ferroelectrics* 89 1989: pp. 1 – 5.
2. **Hosono, Y., Harada, K., Yamashita, Y.** Crystal Growth and Electrical Properties of Lead-Free Piezoelectric Material $(Na_{1/2}Bi_{1/2})TiO_3$–$BaTiO_3$ *Japanese Journal of Applieed Physics* 40 2001: pp. 5722 – 5726.
3. **Suchanicz, J., Kusz, J., Bhöm, H., Duda, H., Mercurio, J. P., Konieczny, K.** Structural And Dielectric Properties Of $(Na_{0.5}Bi_{0.5})_{0.70}Ba_{0.30}TiO_3$ Ceramics *Journal of the European Ceramic Society* 23 2003: pp. 1559 – 1564.
4. **Gomah-Pettry, J. R., Saïd, S., Marchet, P., Mercurio, J. P.** Sodium-Bismuth Titanate Based Lead-Free Ferroelectric Materials *Journal of the European Ceramic Society* 24 2004: pp. 1165 – 1169.
5. **Xu, Q., Chen, S., Chen, W., Wu, S., Zhou, J., Sun, H., Li, Y.** Synthesis And Piezoelectric And Ferroelectric Properties Of $(Na_{0.5}Bi_{0.5})_{1-x}Ba_xTiO_3$ Ceramics *Materials Chemistry and Physics* 90 2005: pp. 111 – 115.
6. **Pronin, I. P., Syrnikov, P. P., Isupov, V. A., Egorov, V. M., Zaitseva, N. V.** Peculiarities Of Phase Transitions In Sodium-Bismuth Titanate *Ferroelectrics* 25 1980: pp. 395 – 397.
7. **Chu, B.-J., Cho, J.-H., Lee, Y.-H., Kim, B.-I., Chen, D.-R.,** The Potential Application of BNT-based Ceramics in Large Displacement Actuation *Journal of Ceramics Processing Research* 3 2002: pp. 231 – 234.
8. **Zhao, S., Li, G., Wang, T., Yin, Q.** Ferroelectric and Piezoelectric Properties of $(Na,K)_{0.5}Bi_{0.5}TiO_3$ Lead Free Ceramics *Journal of Physics D: Applied Physics* 39 2006: pp. 2277 – 2281.
9. **Miura, K., Tanaka, M.** Origin of Fatigue in Ferroelectric Perovskite Oxides *Japanese Journal of Applieed Physics* 30 1996: pp. 2719 – 2725.
10. **Singh, D. J., Ghita, M., Halilov, S. V., Fornari, M.** The Role of Pb in Piezoelectrics and Possible Substitutions for it *Journal de Physique IV Fr.* 128 2005: pp. 47 – 53.

11. **Nagata, H., Takenaka, T.** Additive Effects on Electrical Properties of $(Bi_{1/2}Na_{1/2})TiO_3$ Ferroelectric Ceramics *Journal of the European Ceramic Society* 21 2001: pp. 1299 – 1302.
12. **Herabut, A., Safari, A.** Processing and Electromechanical Properties of $(Bi_{0.5}Na_{0.5})_{1-x}La_xTiO_3$ Ceramics *Journal of American Ceramic Society* 80 1997: pp. 2954 – 2958.
13. **Wang, X. X., Chan, H. L. W., Choy, C. L.** $(Bi_{0.5}Na_{0.5})_{0.94}Ba_{0.06}TiO_3$ Lead-free Ceramics with Simultaneous Addition of CeO_2 and La_2O_3 *Applied Physics A* 80 2005: pp. 333 – 336.
14. **Kumari, K., Prasad, K., Chandra, K. P., Yadav, K. L., Sen, S.** Structural and Dielectric Properties of ZrO_2 Added $(Na_{1/2}Bi_{1/2})TiO_3$ Ceramic *Brazilian Journal of Physics* 39 2009: pp. 297 – 300.
15. **Takenaka, T., Nagata, H.** $(Bi_{1/2}Na_{1/2})TiO_3$-$BaTiO_3$ System for Lead-free Piezoelectric Ceramics *Japanese Journal of Applieed Physics* 30 1991: pp. 2236 – 2239.
16. **Guo, Y., Kakimoto, K.-I., Ohsato, H.** $(Na_{0.5}K_{0.5})NbO_3$–$LiTaO_3$ Lead-free Piezoelectric Ceramics *Materials Letters* 59 2005: pp. 241 – 244.
17. **Li, Y. M., Chen, W., Zhou, J., Xu, Q., Gu, X. Y., Liao, R. H.** Impedance Spectroscopy and Dielectric Properties of $Na_{0.5}Bi_{0.5}TiO_3$–$NaNbO_3$ Ceramics *Physica B* 365 2005: pp. 76 – 81.
18. **Zhou, C.-R., Liu, X.-Y.** Dielectric Properties and Relaxation of $Bi_{0.5}Na_{0.5}TiO_3$–$BaNb_2O_6$ Lead-free Ceramics *Bulletin of Material Science* 30 2007: pp. 575 – 578.
19. **Liu, X.-Y., Zhou, C.-R., Shan, Z.-H.** Depolarization Temperature and Piezoelectric Properties of $Na_{1/2}Bi_{1/2}TiO_3$–$Na_{1/2}Bi_{1/2}(Zn_{1/3}Nb_{2/3})O_3$ Ceramics by two-stage Calcination Method *Bulletin of Material Science* 30 2007: pp. 579 – 581.
20. **Prasad, K., Kumari, K., Lily, Chandra, K. P., Yadav, K. L., Sen, S.** Glass Like Response of $(Na_{1/2}Bi_{1/2})TiO_3$-WO_3 Ceramic *Solid State Communications* 144 2007: pp. 42 – 45.
21. **Williamson, G. K., Hall, W. H.** X-ray Line Broadening from Filed Aluminum and Wolfram *Acta Metallurgica* 1 1953: pp. 22 – 31.
22. **Gabriel, C., Gabriel, S., Grant, E. H., Halstead, B. S. J., Mingos, D. M. P.** Dielectric Parameters Relevant to Microwave Dielectric Heating *Chemical Society Revievs* 27 1998: pp. 213 – 223.

DOI: 10.5755/j02.ms.26086